Aberrant immune regulation and enrichment of stem-like CD8$^+$ T cells in the pancreatic lymph node during type 1 diabetes development

Running title: Stem-like CD8$^+$ T cell phenotypes enriched in T1D

Leeana D. Peters[1, 2], Maigan A. Brusko[1, 2], Howard R. Seay[1, 2], Amanda L. Posgai[1, 2], Clive H. Wasserfall[1, 2], Mark A. Atkinson[1, 2, 3], Rhonda Bacher[2, 4], and Todd M. Brusko[1, 2, 3, 5]*

[1]Department of Pathology, Immunology, and Laboratory Medicine, College of Medicine, University of Florida, Gainesville, FL, USA

[2]Diabetes Institute, University of Florida, Gainesville, FL, USA

[3]Department of Pediatrics, College of Medicine, University of Florida, Gainesville, FL, USA

[4]Department of Biostatistics, College of Public Health and Health Professions, University of Florida, Gainesville, FL, USA

[5]Department of Biochemistry and Molecular Biology, College of Medicine, University of Florida, Gainesville, FL, USA

*Correspondence to: Todd M. Brusko, Ph.D., Department of Pathology, Immunology and Laboratory Medicine, College of Medicine, University of Florida, 1275 Center Drive, Biomedical Sciences Building J589, Box 100275, Gainesville, FL 32610. E-mail address: tbrusko@ufl.edu. TEL: (352) 273-9255. FAX: (352) 273-9339.

Conflict of Interest Statement: The authors declare no relevant conflicts of interest related to the work presented in this manuscript.

Word Count: 10286, Tables: 5, Figures: 5, Supplementary Tables: 4, Supplementary Figures: 8

Summary

Effector $CD8^+$ T cells are key cellular drivers of type 1 diabetes (T1D) pathogenesis, yet questions remain regarding the molecular defects leading to altered cytotoxicity, their signature in peripheral tissues, and their receptor specificity. Thus, we analyzed human pancreatic lymph nodes (pLN) using mass cytometry and single cell RNA sequencing (scRNAseq) with combined proteomic and T cell receptor (TCR) profiling. Cytometric analysis revealed an enriched population of T stem-cell memory (Tscm)-like cells ($CD8^+CD45RA^+CD27^+CD28^+CCR7^+CXCR3^+$ T cells) in T1D pLNs. scRNAseq profiling indicated an elevated inflammatory cytokine gene signature (*IFITM3*, *LTB*) along with regulators of terminal differentiation (*BCL6*, *BCL3*) in naïve $CD8^+$ T cells in T1D pLN, while effector $CD8^+$ T cells expressed features of progenitor exhausted cells (*BCL2*). Immune Response Enrichment Analysis (IREA) indicated IL-15 signaling as a significant driver of these phenotypes. Integrated TCR and transcriptomic analysis revealed a cluster of diverse naïve-like $CD8^+$ T cell clones in T1D pLN. When comparing pLN and pancreatic cellular slice extracts, we observed sharing of effector $CD8^+$ T cells, with upregulation of terminal effector signatures detected within the pancreas relative to paired pLN samples. Thus, we provide multimodal cellular profiles enriched in T1D tissues for consideration in therapeutic targeting.

Keywords: type 1 diabetes, human, pancreas, lymph node, CD8 T cell, single cell RNA sequencing

41 **Introduction**

42 Genetic fine mapping studies have identified that type 1 diabetes (T1D)-associated risk variants
43 preferentially localize to enhancer regions within immune cells, namely T and B cells[1]. However,
44 inaccessibility of the pancreas from living individuals mandates that studies examining immune cell
45 function in T1D largely be derived from peripheral blood, which may not accurately reflect phenotypes
46 within the target organ during disease pathogenesis. Identifying the molecular basis for T1D-associated
47 immune dysregulation within the pancreas and pancreatic draining lymph nodes (pLN) is highly valuable
48 in the process of developing targeted therapies.

49 The role of the pLN in promoting T1D progression is incompletely characterized, but murine and
50 human studies have implicated the pLN as an important priming site for immune activation[2-4]. In the
51 non-obese diabetic (NOD) mouse model of T1D, pLN self-renewing autoreactive T cells were found to be
52 an important source of islet antigen-specific cytotoxic lymphocytes[5]. Human studies indicate that
53 patients with T1D possess skewed T cell subset distributions within the pLN, with reduced T follicular
54 regulatory (TFR) cell frequency reported in one study[6] and increased Th17 cells noted in another[7].
55 Although there are conflicting reports as to whether deficits in circulating regulatory T cell (Treg)
56 number and function are present in T1D patients[8, 9], multiple studies have demonstrated deficits in
57 suppressive capacity[7] and migration toward the pancreas[10] in Tregs derived from T1D pLN.

58 Though peripheral blood signatures do not always correlate with those from tissues[11], there
59 have been many important knowledge gains linking peripheral immunological signatures to clinical
60 outcomes. Interestingly, many of the signatures associated with immunotherapeutic response have
61 converged around $CD8^+$ T cell subsets. For example, an exhausted-like $CD8^+$ population expressing
62 negative regulatory molecules, including TIGIT and PD-1, together with exhaustion markers KLRG1 and
63 CD57, was associated with C-peptide preservation post-treatment with alefacept (LFA3-Ig)[12]. Similarly,
64 expansion of $TIGIT^+KLRG1^+CD8^+$ T cells was found preferentially in those who responded to teplizumab

65 (α-CD3)[13]. Moreover, studies in mice[5] and humans[14, 15] have implicated $CD4^+$ and $CD8^+$ stem cell memory
66 T cells (Tscm) as a potentially important reservoir for promoting pathogenic antigen-specific responses
67 in T1D. Although clinical studies have shown that exhausted-like populations are clonally related to a
68 different $CD8^+$ memory population expressing more activation markers relative to exhaustion markers[12],
69 there is a paucity of information in T1D regarding the distribution of these subsets in secondary
70 lymphatic organs and pancreas, their receptor profiles, or the pathways driving these phenotypes.

71 Our lab has previously generated sorted T cell receptor (TCR) profiles from donor-matched pLN,
72 spleen, and peripheral blood samples, revealing cell type-dependent repertoire sharing across tissues,
73 with $CD8^+$ T cells demonstrating the greatest degree of sharing[16]. The advent of single cell profiling
74 technologies enables the examination of sharing between lymph node and pancreas T cell populations
75 with greater resolution. To understand the phenotypic and transcriptomic profile of immune cell
76 populations in disease-relevant tissues, we performed single cell multi-omic analysis of the pLN as well
77 as pancreatic T cells from donors with and without T1D. In this study, we show that circulating
78 phenotypic signatures previously identified to correlate with T1D status or immunotherapeutic response
79 are shared across tissue immune phenotypes. Moreover, we offer evidence that human $CD8^+$ T cells
80 possess less differentiated phenotypes in the pLN in T1D and that effector populations differentiate
81 further upon trafficking to the pancreas.

82 **Methods**

83 **Human Organ Donors**

84 Tissues were recovered from T1D donors, donors possessing islet autoantibody positive (AAB+) as well
85 as donors without diabetes, and negative for islet autoantibodies (ND) according to the Network for
86 Pancreatic Organ donors with Diabetes (nPOD) inclusion criteria[17]. Demographic information used to
87 stratify subjects for analyses was obtained from the nPOD datashare (https://npoddatashare.coh.org/)
88 and nPOD data portal (https://portal.jdrfnpod.org) websites.

89 **Organ Processing**

90 Tissues were processed as previously described[16]. Briefly, pLN were dissociated in HBSS + 10% human
91 (male, type AB) serum (Atlanta Biologicals) using a gentleMACS tissue processor (Miltenyi), followed by
92 subsequent homogenization and filtering steps using a tissue douncer (40 mL; loose pestle; Wheaton)
93 and 100-µm, 70-µm, and 30-µm filters (Miltenyi) to obtain a single cell suspension. Cells were freshly
94 analyzed by flow cytometry as described below, and remaining cells were cryopreserved using CryoStor
95 CS10 (Stemcell). Live pancreatic slices were prepared from nPOD organ donors as previously described[18]
96 and freshly digested with 1X collagenase IV (Stemcell) diluted in DMEM for 30 minutes at 37°C and 5%
97 CO_2. Remaining tissue was gently mechanically dissociated with frosted slides and filtered using 70-µm
98 filters (Miltenyi) to obtain a single cell suspension. Cells were enriched for $CD45^+$ cells using CD45
99 Microbeads (Milltenyi) and processed for scRNAseq (10X Genomics) as below.

100 **Flow Cytometry**

101 Fresh tissues were dissociated as above and stained with Live/Dead yellow viability dye (Invitrogen) and
102 incubated with TruStain FcX (Biolegend) according to manufacturer's instructions prior to staining with a

103 panel of antibodies broadly examining memory, effector, and naïve immune cell phenotypes (**Table 1**)
104 consistent with previously published methods[19]. Data were acquired on an LSRFortessa (BD) and
105 analyzed using FlowJo V10.8.2 software.

106 **Mass Cytometry**

107 Cryopreserved cells from pLN of ND (n=12) and T1D donors (n=10) were stained with a 35-marker panel
108 (**Table 2**) of MAXPAR metal-chelating polymers and run on a CyTOF mass cytometer by the Human
109 Immune Monitoring Center at Stanford University, as reported previously[20].

110 **Mass Cytometry Analysis Pipeline**

111 Data were normalized between batches using premessa[21] in R based on internal bead controls. After
112 this, FCS files were loaded into FlowJo (BD Biosciences), beads were excluded, and live single $CD45^+$ cells
113 were used for downstream analysis. Data analysis involved importing FCS files into R and creating a
114 flowset using the flowCore package[22]. Data were arcsinh transformed with a cofactor of 5 prior to using
115 the expression data and cell metadata to create a Seurat object. PCA was run using all panel markers,
116 after which K nearest neighbors (KNN) were calculated using FindNeighbors(), and initial clustering using
117 the lovain algorithm was performed (resolution=0.2). PCA was re-run on subsetted data with markers
118 not associated with the lineage of interest removed. Nearest neighbors were calculated as above and
119 subclustering was performed as above for each subset using the Louvain algorithm (resolution=0.5). Cell
120 counts per cluster per individual were determined and normalized by the total number of cells to allow
121 for comparison of cluster proportions. Differential abundance analysis was performed using propeller[23]
122 with age and batch as covariates in a linear model designed with model.matrix(~0 + group + age +
123 Batch). Design matrix and contrasts (T1D-ND) were incorporated into the propeller.ttest function with
124 arguments robust=T, trend=F, sort=T. Differential expression analysis was performed using the mean

125 expression values of each marker per cluster as input into a linear model using limma. Briefly, the design
126 matrix as defined with model.matrix(~condition + batch) was input alongside mean marker expression
127 into the lmFit function, the output of which was fed into the eBayes function. Significantly altered
128 cluster proportions or expression values were defined as Bonferroni adjusted p-value <0.05.

129

130 **Single Cell RNA Sequencing**

131 Cryopreserved single cell suspensions were thawed and stained with a cocktail of 7 oligo-barcoded
132 TotalSeq antibodies (Biolegend, **Table S1**) to aid in clustering naïve and memory $CD8^+$ and $CD4^+$ T cell
133 phenotypes. Prior to use, Totalseq antibodies were centrifuged at 14000x*g* for 10 minutes at 4°C to
134 avoid antibody aggregates, as recommended by the manufacturer. Cell viability was assessed using
135 acridine orange and propidium iodide (AO/PI) staining on a Nexcelom Cellometer or CellDrop. For six
136 samples with viability <70%, the Dead Cell Removal Kit (Stemcell) was used. $1x10^6$ cells per sample
137 (viability >70%) were resuspended in 100µL volume of PBS + 1% BSA and stained with TruStain FcX
138 (5µL/test) to block Fc receptors for 10 minutes at 4°C prior to incubation with the antibody master mix
139 (0.5µL of each antibody/test) for 30 minutes at 4°C. Cells were washed four times with 3mL of chilled
140 PBS + 1% BSA, after which live cells were counted using AO/PI on a Nexcelom Cellometer or CellDrop
141 and volumes adjusted to obtain a targeted recovery of 10,000 cells. Single cell suspensions were loaded
142 into the Chromium Controller (10X Genomics) and libraries prepared according to the 5' v1.1, 5' v2, and
143 5' HT v2 kit protocols (10x Genomics). Libraries were sequenced on an Illumina Novaseq or Novaseq X
144 instrument with a target of 50,000 paired reads for gene expression, 10,000 paired reads for surface
145 protein, and 5,000 paired reads for TCR libraries. Median gene expression library sequencing saturation
146 was 80.9%.

147 **Single Cell Read Processing**

148 BCL files were processed to fastq files using the cellranger mkfastq pipeline (10X genomics). Fastq files
149 from gene expression, surface protein, and TCR libraries were processed to matrices using the cellranger
150 multi (10X genomics) count pipeline in order to maximize counting of cells with all three modalities.

151 **Single Cell RNAseq Normalization and Analysis Pipeline**

152 scRNAseq data were subject to quality control (QC) by removing doublets using the doubletfinder
153 package[24], and cells were removed based on cutoffs of reads/cell ≤2000 and percent mitochondrial
154 reads ≤10%, then normalized using the DSB package[25] to remove background noise and ambient signal.
155 After this initial filtering, data were log normalized with NormalizeData() and scaled with ScaleData(),
156 then variable features were calculated and dimensionality reduction was performed in Seurat[26]. For the
157 antibody-derived tag data, variable features were set to all antibodies included, data were scaled[26], and
158 principal component analysis (PCA) was run. Data were integrated in Seurat using IntegrateLayers() with
159 RPCA as the integration method. Integration of TCR with gene expression data was performed using
160 scRepertoire[27] in R. Clones were defined as sequences sharing an identical complementarity determining
161 region 3 (CDR3) for both TCRα and TCRβ. Differentially expressed genes (DEGs) were calculated using
162 MAST[28] with sex as a latent variable with a minimum expression threshold of 0.10 and reported when
163 false discovery rate (FDR) corrected $p<0.05$ and log2 fold change (FC)≥0.26. Pathway enrichment
164 analyses were performed using the top 100 most differentially expressed genes between T1D and ND
165 donors with FDR $p<0.05$ per cluster ranked by log2FC as input into the ReactomePA[29] package for pLN,
166 and the R package escape[30] was used to perform single-sample Gene Set Enrichment Analysis (ssGSEA)
167 using the integrated pancreas and pLN dataset. Results were reported when Benjamini-Hochberg
168 corrected $p<0.1$ as noted in figure legends.

169 **Clonotype Neighbor Graph Analysis (CoNGA)**

170 The RNA assay from the integrated pLN Seurat object was exported in h5ad format for python. Filtered
171 contig annotation data from each sample was merged using make_10x_clones_file_batch from the
172 conga package in python. The resulting merged TCR data were used along with the gene expression data
173 as input for run_conga.py[31] with the –all flag and batch keys set to status and nPOD identification
174 number (ID) in order to compare the composition of clusters by clinical status and across all donors.
175 Gene expression data were also batch corrected using the argument batch_integration_method
176 harmony with batch_integration_key batch. Clone information was added to the Seurat object metadata
177 in order to allow visualization of TCR clusters on the existing gene expression Uniform Manifold
178 Approximation and Projection (UMAP). Clones that possessed a conga score<1, indicative of significant
179 overlap between gene expression and TCR neighborhoods beyond what would be expected by chance[31],
180 were used as input to evaluate enrichment in cluster composition by clinical status using two-sided
181 Fisher's exact test as reported in the figure legend.

182 **Sex as a biological variable**

183 Male and female organ donors were accepted in this study, without biological sex considered as a major
184 covariate in T1D and ND donors.

185 **Statistics**

186 Data were analyzed using R v4.2.3, python v3.9 and GraphPad Prism v9. Statistical tests and p-values are
187 reported in the figure legends.

188 **Study approval**

189 The study was conducted in accordance with federal guidelines and the University of Florida (UF)
190 Institutional Review Board approved protocol IRB201600029, as previously described[32].

191 **Data availability**

192 Mass cytometry and flow cytometry data are available at ImmPort (https://www.immport.org, accession
193 number: SDY3066. Supporting Data Values associated with this manuscript are provided in the
194 supplement. Gene expression and TCR data are available on GEO with accession: In Progress

195 **Results**

196 **Mass cytometry reveals a population of CD8$^+$CXCR3$^+$ T cells enriched in T1D pLN**

197 The diverse nature of immune cell phenotypes mandates the use of high-parameter technologies, such
198 as cytometry time of flight (CyTOF)[33, 34 12], to deep-phenotype multiple immune subsets. We applied
199 high-parameter CyTOF (35 markers, **Table S2**) to pLN derived from 10 T1D and 12 ND nPOD organ
200 donors (**Table 2; Figure 1A**). Clustering total CD45$^+$ immune cells revealed 11 unique populations
201 spanning B cells, CD4$^+$ T cells, CD8$^+$ T cells, myeloid, and natural killer (NK) cells (**Figure 1B**). We observed
202 no significant differences in cluster abundance globally between T1D and ND donors (**Figure S1A-B**);
203 however, differential expression analysis revealed significantly enhanced CXCR3 expression in cluster 4,
204 a naïve CD8$^+$ T cell cluster (p=0.04, fold change [FC]= 2.43), in T1D pLN as compared to ND donors
205 (**Figure 1C-D**). We confirmed these findings in an independent cohort of 24 nPOD pLN donors comprised
206 of ND, autoantibody positive (AAB+) and T1D donors (**Table 3**) using flow cytometry (**Figure S2**).

207 We then performed subclustering to obtain a finer resolution of immune cell subsets from the
208 CyTOF data. As one batch demonstrated slight, non-significant differences in age (**Figure S3**), we chose
209 to examine differences in cluster proportions using a linear model with age and batch incorporated as
210 covariates. Subsetting and reclustering of B cells and CD4 T cells yielded no significant changes in cluster
211 abundance or marker expression by clinical status (**Figure S4**). However, CD8$^+$ T cell subclustering
212 yielded eight proteomic clusters (**Figure 2A-B**), with a T1D-associated increase in the proportion of CD8$^+$
213 T cell cluster 0, expressing the naïve T cell markers CD45RA and CCR7, costimulatory molecules CD27
214 and CD28, as well as low levels of the chemokine receptor CXCR3, which confers migratory capacity
215 towards CXCL10[35] (**Figure 2C**). This finding was also confirmed in the aforementioned independent flow
216 cytometry cohort (**Figure 2D, Table 3**), where T1D donors possessed a significantly increased proportion
217 of CXCR3$^+$ cells within the naïve (CD45RA$^+$CCR7$^+$) CD8$^+$ T cell compartment as compared to both ND

218 (p=0.0053, FC=2.70) and islet autoantibody positive (AAB) donors (p=0.0062, FC=5.08). We next
219 compared the differentiation status of these cells, as CXCR3 expression may indicate a Tscm
220 phenotype[36], while CXCR5 expression is associated with precursor exhausted and differentiated effector
221 memory cells[37, 38]. When comparing CXCR3 and CXCR5 expressing CD8 T cell populations, $CXCR3^{+}CXCR5^{+}$
222 memory $CD8^{+}$ T cells expressed increased PD-1 as compared to their $CXCR3^{+}CXCR5^{-}$ counterparts,
223 supporting a less terminal phenotype for single $CXCR3^{+}$ cells (**Figure S5A-B**). Importantly, these
224 phenotypic signatures are clinically relevant in peripheral blood studies: we recently reported a T1D-
225 associated increase in $CXCR3^{lo}$ naïve $CD8^{+}$ T cells[19], and circulating $CD8^{+}$ T cells with a more terminally
226 differentiated/exhausted profile have been previously correlated with preservation of C-peptide and
227 response to teplizumab[12, 13]. Collectively, these data and our prior peripheral blood findings[39] suggest
228 Tc1 skewing as an immunological feature of T1D shared across tissues.

229 **IL-15 drives memory maintenance and averts the exhaustion program in T1D $CD8^{+}$ T cells**

230 To explore the transcriptomic profile of the cell populations previously identified by both CyTOF and
231 fluorochrome-based flow cytometry, we performed single cell RNA sequencing (scRNAseq) analysis with
232 TCR-seq on donor pLN (**Figure 3A**). After QC, we obtained 122,300 cells across 16 individuals (9 T1D, 7
233 ND) (**Table 4**) that comprised 25 clusters spanning $CD4^{+}$ T cells, $CD8^{+}$ T cells, B cells, NK cells, innate
234 lymphoid cells (ILCs), monocyte/macrophages and dendritic cells (DCs) (**Figure 3B**, **Figure S6A-B**). No
235 significant differences in global cluster abundance across clinical status were detected (**Figure S6C-D**).
236 We performed subclustering to more deeply examine alterations in T cell phenotype, yielding 15
237 subclusters spanning naïve, memory, and exhausted T cells, as well as Tregs (**Figure 3C**). Differential
238 expression analysis of T1D compared to controls identified conserved signatures across multiple CD4 T
239 cell clusters, such as a reduction in genes responsible for negative regulation of cytokine signaling (e.g.,
240 *TNFAIP3*[40] within naïve CD4, T follicular helper [TFH], Th17, thymic Treg [tTreg] clusters) and

241 activation/proliferation (e.g., *JUND*[41] within TFH, tTreg, Th1/17, Th17 clusters), as well as a broad
242 increase in interferon signaling genes (e.g., *IFITM3*[42] within Th17, naïve CD4, exhausted CD4, activated
243 naïve CD4, cycling CD4, TFH, Th1/17) (**Table S3**).

244 We next focused more deeply on $CD8^+$ T cell subsets as these phenotypes were significantly
245 altered in our CyTOF and flow cytometry data. When comparing differentially expressed genes (DEGs;
246 defined as false discovery rate (FDR) corrected $p_c<0.05$ and Log2FC≥0.26) between T1D and ND pLN, we
247 observed within the naïve $CD8^+$ T cell cluster (**Figure 3D**) an upregulation of genes involved in
248 inflammatory cytokine signaling (*IFNAR2*[43], *IFNGR2*[44], *IFITM3*, *LTB*[45], *SOCS3*[46], *IL32*[47], *IL27RA*[48]) as well as
249 regulators of terminal differentiation (*BCL3*[49], *BCL6*[50], *BATF*[51]). Moreover, naïve $CD8^+$ T cells from T1D
250 donors also downregulated genes involved in negative regulation of cytokine signaling (*TNFAIP3*[40],
251 *SOCS1*[52]) and genes associated with T cell exhaustion (*DUSP2*[53], *NR4A2*[54], *TSC22D3*[55]) as compared with
252 ND. In the CD8 effector T cell (Teff) cluster (**Figure 3D**), we observed an upregulation of genes involved
253 in effector function (*SLC3A2*[56], *NKG7*[57], *HOPX*[58]), as well as migratory genes (*VIM*[59], *ITGA1*[60]) in T1D
254 relative to ND donors. We also noted upregulation of the anti-apoptotic factor *BCL2*, which is important
255 for the maintenance of long-lived memory subsets[61, 62], within CD8 Teff in T1D. Moreover, within this
256 cluster, we observed downregulation of genes associated with terminal differentiation and exhaustion
257 (*CXCR4*[63], *DUSP2*[53], *NR4A1*[54]), indicative of restraining of terminal differentiation in T1D as compared to
258 controls. Similarly, in the exhausted CD8 T cell cluster (CD8 Texh) (**Figure 3D**), we observed upregulation
259 of genes involved in chemotaxis (*XCL2*[64]), calcium signaling (*S100A6*, *S100A11*[65]), and inflammatory
260 cytokine response (*IL21R*[66], *IFITM1*, *IFITM3*, *IFITM2*[42, 67]), while genes associated with terminal
261 differentiation and exhaustion (*TSC22D3, DUSP2*, *HLA-DQB1*[68]) were downregulated in T1D.

262 Accordingly, pathway analysis using the Reactome database revealed that naïve CD8 T cells
263 (**Figure 3E**) in T1D were enriched for interleukin signaling and interferon signaling, while CD8 Teff (**Figure**
264 **3F**) were enriched for interleukin signaling and smooth muscle contraction, the latter likely reflective of

265 increased calcium signaling (*ANXA1*, *ANXA2*)[69]. Lastly, CD8 Texh (**Figure 3G**) were enriched for interferon
266 signaling, IL-21 signaling, and apoptotic processes, though the latter is likely reflective of negative
267 regulation of apoptosis, as upregulated genes *S100A11*[70], *ANXA2*[70, 71], and *VIM*[72] are involved in
268 inhibition of apoptosis, while *LMNA* is involved both in inhibiting apoptosis[73] and enhancing T cell
269 activation[74]. We then performed Immune Response Enrichment Analysis (IREA), which uses an extensive
270 database of specific gene sets induced by cytokine treatment[75], to infer the cytokine milieu driving these
271 CD8 phenotypes. Across the trajectory of $CD8^+$ T cell differentiation, signatures were significantly
272 enriched for IL-15 signaling in T1D (**Figure 3H-J**), which is known to promote stemness and restrain
273 exhaustion-like phenotypes[76] and can synergize with other inflammatory cytokines to promote effector
274 function[77].

275 **$CD8^+$ T cell clones possessing a naïve-like phenotype are more prevalent in T1D pLN**

276 Individual analyses of receptor or transcriptomic data may preclude insights into the relationships
277 between repertoire characteristics and phenotype. Thus, recent methods have been developed to
278 enable joint analysis of these modalities, namely Clonotype Neighbor Graph Analysis (CoNGA)[31], which
279 has shown utility in revealing transcripts associated with specific TCR genes and features. We applied
280 CoNGA (**Figure 4A**) to our pLN dataset, which identified 35 groups with significant (CoNGA score <1)
281 overlap in TCR and gene expression neighborhoods in pLN as indicated by CoNGA score and a minimum
282 of 4 cells per group (**Figure S7**). We overlaid CoNGA scores on the previously computed gene expression
283 data and observed that the most significant hits were localized to naïve $CD8^+$, mucosal-associated
284 invariant T (MAIT)/tissue resident memory T (TRM), and $CD8^+$ Teff cell clusters (**Figure 4B**). Clustering
285 using the gene expression data only using CoNGA yielded 16 unique clusters (**Figure 4C**), while clustering
286 using the TCR data only yielded 20 unique clusters (**Figure 4D-E**). We observed that CoNGA clone hits
287 belonging to CoNGA gene expression (GEX) cluster 10 and TCR cluster 3 were found in several T1D

288 donors, the highest frequency being found in new-onset donor 6550, while 32/33 clones detected in ND
289 donors (96%) were found in a single ND donor (**Table S4**). Thus, clones belonging to these clusters were
290 more often found in T1D (p=0.0033, OR=1.878) (**Figure 4F**). Among the clusters with >21 clones (0.1% of
291 unique clones from the dataset), we obtained 11 joint gene expression and TCR clusters. In accordance
292 with the original publication[31], we found a stronger relationship between receptor and phenotypes in
293 $CD8^+$ T cells and invariant T cells, with all of our CoNGA hit clusters being comprised of $CD8^+$ T cells,
294 including naïve, effector, T resident memory (TRM) and MAIT cell clusters (**Figure 4G**). The enriched GEX
295 cluster 10/TCR cluster 3 is comprised of $CD8^+$ T cells with high TCR diversity and with high expression of
296 *CCR7*, *SELL*, and *IL7R*. The TCRs within this cluster possessed a diverse TCR beta chain (*TRB*) repertoire,
297 while alpha chain gene usage was restricted to TRAV14/DV4, TRAV38-2/DV8, and TRAV38-1 (**Figure 4G**).
298 Additionally, this cluster also possessed a low Atchley factor 4 score (blue af4 logo, TCRseq features
299 panel, **Figure 4G**), which has previously been associated with larger, more hydrophobic residues[31].
300 Interestingly, we also noted an increase (p=0.0180, OR=1.792) in a group of expanded TCRs (CoNGA
301 gene expression cluster 15 paired with TCR cluster 14) comprised of MAIT and semi-invariant T cells
302 (TRAV1-2 gene usage paired with a more diverse set of TRB chains) in T1D pLN (**Figure S8**).

303 **Shared memory T cell populations demonstrate enhanced effector phenotype in pancreatic slices**

304 To investigate receptor sharing and gene expression across tissues, we performed scRNAseq on isolated
305 immune cells from fresh pancreatic slices[78, 79] and paired pLN (**Figure 5A**) from 2 recent-onset T1D
306 donors (nPOD 6551, duration 0.58 years; nPOD 6536, duration 4 years) with independently confirmed
307 insulitis[80]. Data integration yielded 17 clusters, which included naïve, memory, and effector $CD4^+$ and
308 $CD8^+$ T cell populations, Tregs, B cells, and resident macrophage populations (**Figure 5B**). We first
309 interrogated the TCR repertoire to examine sharing of T cell clones across these tissues, and while both
310 donors possessed insulitis, the newer onset donor 6551 possessed more extensive insulitis than donor

311 6536 (**Figure 5C**). We found that expanded clones localized mostly to clusters 0 (CD8 Teff) and 2 (CD8
312 CTL), respectively corresponding to $CD8^+$ T cell populations with lower and higher expression of
313 cytotoxicity-related molecules (*GZMK*, *CST7*, *LTB*) (**Figure 5D-E**). Clone sharing across pancreas and pLN
314 was minimal, with morisita horn (MH) values of 0.007 and 0.002 for cross-tissue overlap for donors 6536
315 and 6551, respectively (**Figure 5F**). However, even with our limited sample size, we were able to detect 6
316 unique clonotypes shared across tissues and clusters (**Figure 5G, Table 5**). While an expanded $CD4^+$ T cell
317 clone in donor 6536 was shared between tissues (cluster 9, $ICOS^{hi}$ TCM), the majority of sharing was
318 detected between the effector CD8 clusters 0 and 2, especially within donor 6551 as compared to donor
319 6536, perhaps due to reduced infiltration as a result of increased disease duration.

320 We next investigated tissue-specific phenotypic differences in these clusters. We noted that
321 $CD8^+$ Teff clusters 0 and 2, defined by expression of NK cell receptors (*KLRK1*[81], *KLRB1*[82]), Th1 related
322 chemokine receptors and ligands (*CXCR3*, *CXCR6*, *CCL5*[83]) and markers of terminally differentiated
323 memory subsets (*LAG3*, *KLRD1*, *EOMES*[84]), were the most commonly shared clusters across tissues, while
324 less differentiated subsets, such as naïve T cells, were expectedly more prevalent in pLN and
325 inflammatory macrophages more prevalent in pancreas (**Figure 5H**). Examining DEGs of total CD8 T cells
326 between tissues revealed increased expression of genes involved in promoting naïve/stem-like
327 phenotypes, *LEF1* (Log2FC=4.8, $p_{adj}=1.6e^{-7}$) and *SELL* (Log2FC=4.0, $p_{adj}=1.4e^{-}7$), in pLN relative to
328 pancreatic slice (**Figure 5I**). As this could partially be explained by the increased proportion of naïve cells
329 in pLN relative to pancreatic slice, we sought to compare gene expression of shared populations across
330 tissues. We found that cells from cluster 0 (CD8 Teff) derived from pancreatic slices expressed enhanced
331 markers of cytotoxicity such as *GZMB* (Log2FC=5.46, $p_{adj}=1.4e^{-46}$) as well as exhaustion marker *DUSP4*[85]
332 (Log2FC=6.6, $p_{adj}=1.3e^{-57}$) alongside reduced expression of common gamma chain cytokine receptors
333 *IL7R (*Log2FC=-1.9, $p_{adj}=2.5e^{-10}$) and *IL2RG* (Log2FC=-2.0, $p_{adj}=4.1e^{-5}$) (**Figure 5J**). Cluster 2, which
334 possessed a similar transcriptomic profile to cluster 0 but with enhanced expression of cytotoxicity and

335 memory markers (CD8 CTL), demonstrated similar transcriptomic expression differences as cluster 0
336 across tissues (**Figure 5K**). GSEA of cluster 0 revealed upregulation of inflammatory signaling pathways,
337 namely IL-6-JAK-STAT3 (Log2FC=2.3, p_{adj}=1.5e^{-19}) and TNFα signaling (Log2FC=0.34, p_{adj}=1.7e^{-7}), as well
338 as downregulation of Wnt-Beta catenin signaling (Log2FC=-0.6, p_{adj}=2.3e^{-3}) (**Figure 5L**), altogether
339 suggesting that this cluster acquired a more differentiated transcriptomic program in pancreas relative
340 to pLN. We observed similar upregulation of inflammatory pathways in cluster 2 (**Figure 5M**). Notably,
341 while Wnt-Beta catenin signaling was not significantly enhanced in pLN for this cluster, we did observe
342 upregulation of *GIMAP5*[86] (Log2FC=-3.3, p_{adj}=1.5e^{-8}) in pLN, which is an important negative regulator of
343 GSK3β and thus, potentially enhances Wnt-signaling. Akin to recent reports in NOD mice that precursor
344 diabetogenic T cells are primed and maintained as a self-renewing pool in the pLN, seeding terminally
345 differentiated cells that expand in the islets[5], our data are indicative of distinct tissue programs allowing
346 for maintenance of CD8^{+} T cell populations and prevention of exhaustion in the pLN, as well as
347 acquisition of further effector function in the pancreas during human T1D.

348 **Discussion**

349 Despite tremendous progress in characterizing circulating immune cells in T1D, a critical gap in
350 knowledge remains as to alterations in tissue immune phenotypes. Large datasets derived from the
351 pancreas have given insight into disease-related changes in endocrine[87, 88] composition and
352 function, as well as potential changes in immune:islet cell communication[87, 89], but have limited
353 power to examine immune cell phenotype. Datasets derived from secondary lymphoid organs in
354 T1D are lacking due to the limited availability of samples and, to date, lack receptor information[90].
355 This study begins to address these gaps using complementary methods (i.e., CyTOF,
356 scRNAseq/TCRseq/CITEseq) to assess differences in T cell phenotypes and their potential molecular
357 underpinnings within the pLN and pancreas.

358 $CD8^+$ T cells are classically thought to be a major mediator of islet destruction in T1D, given
359 their abundance in the insulitic lesion[91] and cytolytic function. Moreover, recent studies indicated
360 that $CD8^+$ T cells with a self-renewing phenotype may be important for T1D pathogenesis, as they
361 are elevated in peripheral blood, and autoreactive cells may be biased towards this phenotype[5, 14,
362 92]. Our study shows that $CD8^+$ T cells expressing markers of a Tscm population (CD45RA, CCR7,
363 CXCR3, CD27, CD28) are increased in T1D pLN (**Figures 1-2**). Tscm cells play an important role in
364 memory maintenance and in generating rapidly responding effector cells[93]. It has been previously
365 shown that serum concentrations of cytokines that promote Tscm development, notably IL-15, are
366 enhanced in T1D patients[94, 95]. Moreover, circulating islet antigen-reactive T cells from T1D donors
367 have been shown to possess stem-like features[14]. Enhanced capacity for self-renewal could be
368 clinically detrimental, as multiple therapeutic avenues (e.g., teplizumab, anti-thymocyte globulin
369 [ATG]) have converged on a signature of exhaustion in therapeutic responders[13, 96]. Our study has
370 provided further support for the relevance of this pathway, as IREA analysis revealed an enrichment

371 of IL-15-induced genes across the trajectory of $CD8^+$ T cell differentiation (**Figure 3**). We also
372 observed an increase in cytokine signaling and upregulation of the anti-apoptotic factor *BCL2,*
373 which, coupled with the downregulation of multiple exhaustion-associated genes in this cluster in
374 T1D, could suggest that CD8 T cells favor a progenitor exhausted phenotype rather than a terminal
375 exhaustion phenotype in T1D[61]. Further studies are needed to connect IL-15 signaling in T1D to
376 autoreactive T cell stemness and progenitor exhausted phenotypes and to investigate if inhibiting
377 this pathway may aid in establishing durable tolerance. Notably, baricitinib, an inhibitor of Janus
378 Kinase (JAK) 1/2 signaling and thus, common gamma chain cytokine signaling (including IL-15), has
379 recently demonstrated efficacy in preserving β-cell function in recent-onset T1D donors[97].
380 Interestingly, we observed reduced expression of *IL7R* and *IL2RG* in effector cells derived from the
381 recent-onset T1D pancreas relative to those from paired pLN, indicating that in the pancreas
382 microenvironment, these cells may be more reliant on IL-15 in combination with other effector
383 cytokines, such as IL-21, than IL-2 or IL-7. Whether baricitinib alone could aid in targeting the
384 autoreactive T cell reservoir or if combinatorial therapy will be necessary with T cell exhaustion-
385 inducing therapeutics, such as teplizumab, remains to be seen.

386 Limitations of the study include donor heterogeneity and limited sample size due to the
387 rarity of study tissues. Notably, we were unable to obtain sufficient immune cell numbers from
388 control pancreatic slices to compare immune phenotypes between T1D and ND donors. Our lab is
389 currently utilizing spatial transcriptomic and proteomic technologies to assess this without the need
390 for immune cell isolation. Moreover, T1D is a heterogeneous disease, and it is possible that immune
391 phenotypes identified through our studies may differ across different ancestry groups, which we
392 were not powered to assess. Indeed, though great strides are being made in investigating the
393 genetic drivers of T1D in populations with diverse genetic ancestry[98-100], there are still many

394 knowledge gaps regarding the importance of known genetic risk loci across groups traditionally
395 underrepresented in biomedical research. Despite this, we believe that the information that we
396 have provided using paired phenotype and receptor information for these subsets can be used by
397 the field to identify CDR3 motifs of further interest. As it stands, known TCR sequences that
398 correspond to autoreactive T cell specificity are rare[101]. Moreover, matching sequences to those in
399 curated databases such as the manually curated database of pathology associated sequences
400 (McPAS)[102] and immune epitope database (IEDB)[103] introduces a bias toward known specificities
401 and epitopes of interest. Thus, there is a need to apply new analytical strategies to identify
402 similarities in TCR sequence and transcriptomic features that may indicate a common antigen
403 specificity[104]. We utilized one such tool, CoNGA[31], to examine joint gene expression and receptor
404 features in T1D. This analysis revealed an enrichment of a TCR cluster comprised of diverse naive
405 $CD8^+$ T cells, further supporting our gene expression and proteomic data (**Figure 4**). The feature of
406 low AF4 within this cluster supports previous data wherein autoreactive T cells were found to
407 possess more hydrophobic residues[105], including within autoreactive receptors detected in the
408 pancreas[106].

409 We utilized paired pLN and pancreas T cell data to investigate phenotypes of shared
410 populations and to interrogate whether local expansion of T cells occurred in fresh pancreatic slices.
411 We identified the most abundant shared populations to be effector $CD8^+$ T cells, which were the
412 most clonally expanded populations. Moreover, we noted $CD8^+$ T cells, as a whole, had reduced
413 expression of genes involved in promoting stem-like/naïve phenotypes (*LEF1, SELL*) in pancreas
414 compared to pLN (**Figure 5**). This could be, in part, driven by the local inflammatory milieu. Indeed,
415 we observed enrichment of multiple inflammatory cytokine signaling pathways, namely IL-6 and
416 TNFα, in pancreas relative to pLN T cells, while we observed upregulation of Myc, mTORC1, and

417 Wnt signaling pathways in pLN relative to pancreas T cells. While sharing of TCR clones was limited
418 between donors and difficult to detect due to the sparsity of single cell data, we were able to detect
419 intra-donor sharing of clones across tissues and between clusters. Donor 6551, a 20-year-old donor
420 with 0.58 years disease duration, particularly notable for insulitis severity, possessed expanded
421 $CD8^+$ Teff clones that were shared between tissues and between clusters, whereas in the longer
422 duration (4 years) donor with less insulitis (6536), we were able to detect sharing of only one
423 effector $CD8^+$ clone across clusters and one $CD4^+$ clone across tissues (**Figure 5**). In accordance with
424 murine studies[5], these data support that T cell clones are supplied from the pLN and adopt a more
425 effector and terminally differentiated phenotype in the pancreas during human T1D development.
426 Previously, our lab reported increased circulating $CXCR3^{lo}CD8^+$ T cells in T1D[39] following
427 phenotyping of a cohort of over 824 cross-sectional peripheral blood samples. The present study
428 supports a role for these cells in the draining lymph node, while related terminal effector CXCR3
429 expressing subsets could be found in the target organ. Identifying subsets of interest that are
430 relevant in both peripheral blood and the target organ could aid in efforts to selectively inhibit
431 autoreactivity and monitor outcomes. Importantly, combination CXCR3 antagonism with ACT-777991
432 and α-CD3 treatment leads to disease remission in the NOD mouse[107], and first-in-human trials in
433 healthy adults have shown this compound to be tolerable[108]. Thus, combinatorial strategies to induce
434 tolerogenic phenotypes while targeting pathways relevant to tissue immune phenotypes may represent
435 an avenue to achieve durable tolerance. Taken together, our studies indicate that memory and
436 effector T cell programs in T1D are maintained in the pLN and enhanced locally in the pancreas,
437 likely driven by aberrant regulation of cytokine signaling and impacted by genotype at T1D risk loci.
438 Future directions validating the functionality of clones identified herein and investigating the
439 cellular interactions of $CXCR3^+CD8^+$ T cells across the differentiation trajectory will inform the

440 development of therapeutics to modulate them, providing novel avenues to delay or prevent T1D

441 progression.

Author Contributions

LDP: Designing research studies, conducting experiments, acquiring data, analyzing data, writing the manuscript (original draft), funding acquisition

MAB: Designing research studies, interpreting data, writing the manuscript (reviewing and editing)

HRS: Conducting experiments, acquiring data, writing the manuscript (reviewing and editing)

ALP: Writing the manuscript (reviewing and editing)

EP: Acquiring data, writing the manuscript (reviewing and editing)

CHW: Writing the manuscript (reviewing and editing)

MAA: Writing the manuscript (reviewing and editing), funding acquisition

RB: Analyzing data, writing the manuscript (reviewing and editing), interpreting data

TMB: Designing research studies, interpreting data, writing the manuscript (reviewing and editing), funding acquisition, project oversight

Acknowledgments

We thank the nPOD donors and their families for their important contributions to this research. We also thank the nPOD core team, namely Irina Kusmartseva, Helmut Hiller, and Maria Beery, for their efforts in case acquisition, processing, and distribution.

Funding

This research was conducted with grant support from the National Institutes of Health (NIH) P01 AI042288 to TMB, F31 DK129004 to LDP, as well as from the American Diabetes Association (ADA) 11-23-PDF-78 to LDP, The Leona M. and Harry B. Helmsley Charitable Trust (Grant # 2301-06562). This research was also performed with the support of the Network for Pancreatic Organ donors

with Diabetes (nPOD; RRID:SCR_014641), a collaborative type 1 diabetes research project supported by Breakthrough T1D and The Leona M. & Harry B. Helmsley Charitable Trust (Grant#3-SRA-2023-1417-S-B). The content and views expressed are the responsibility of the authors and do not necessarily reflect the official view of nPOD. Organ Procurement Organizations (OPO) partnering with nPOD to provide research resources are listed at **https://npod.org/for-partners/npod-partners/**.

469 **References**

470 1. Onengut-Gumuscu, S., et al., *Fine mapping of type 1 diabetes susceptibility loci and evidence for*
471 *colocalization of causal variants with lymphoid gene enhancers.* Nat Genet, 2015. **47**(4): p. 381-
472 6.
473 2. Wan, X., et al., *Pancreatic islets communicate with lymphoid tissues via exocytosis of insulin*
474 *peptides.* Nature, 2018. **560**(7716): p. 107-111.
475 3. Turley, S., et al., *Physiological beta cell death triggers priming of self-reactive T cells by dendritic*
476 *cells in a type-1 diabetes model.* J Exp Med, 2003. **198**(10): p. 1527-37.
477 4. Marrero, I., et al., *High-throughput sequencing reveals restricted TCR Vbeta usage and public*
478 *TCRbeta clonotypes among pancreatic lymph node memory CD4(+) T cells and their involvement*
479 *in autoimmune diabetes.* Mol Immunol, 2016. **74**: p. 82-95.
480 5. Gearty, S.V., et al., *An autoimmune stem-like CD8 T cell population drives type 1 diabetes.*
481 Nature, 2022. **602**(7895): p. 156-161.
482 6. Vecchione, A., et al., *Reduced Follicular Regulatory T Cells in Spleen and Pancreatic Lymph Nodes*
483 *of Patients With Type 1 Diabetes.* Diabetes, 2021. **70**(12): p. 2892-2902.
484 7. Ferraro, A., et al., *Expansion of Th17 cells and functional defects in T regulatory cells are key*
485 *features of the pancreatic lymph nodes in patients with type 1 diabetes.* Diabetes, 2011. **60**(11):
486 p. 2903-13.
487 8. Putnam, A.L., et al., *Expansion of human regulatory T-cells from patients with type 1 diabetes.*
488 Diabetes, 2009. **58**(3): p. 652-62.
489 9. McClymont, S.A., et al., *Plasticity of human regulatory T cells in healthy subjects and patients*
490 *with type 1 diabetes.* J Immunol, 2011. **186**(7): p. 3918-26.
491 10. Sebastiani, G., et al., *Regulatory T-cells from pancreatic lymphnodes of patients with type-1*
492 *diabetes express increased levels of microRNA miR-125a-5p that limits CCR2 expression.* Sci Rep,
493 2017. **7**(1): p. 6897.
494 11. Arif, S., et al., *Erratum. Blood and Islet Phenotypes Indicate Immunological Heterogeneity in Type*
495 *1 Diabetes. Diabetes 2014;63:3835-3845.* Diabetes, 2015. **64**(9): p. 3334.
496 12. Diggins, K.E., et al., *Exhausted-like CD8+ T cell phenotypes linked to C-peptide preservation in*
497 *alefacept-treated T1D subjects.* JCI Insight, 2021. **6**(3).
498 13. Long, S.A., et al., *Partial exhaustion of CD8 T cells and clinical response to teplizumab in new-*
499 *onset type 1 diabetes.* Science Immunology, 2016. **1**(5).
500 14. Abdelsamed, H.A., et al., *Beta cell-specific CD8+ T cells maintain stem cell memory-associated*
501 *epigenetic programs during type 1 diabetes.* Nature Immunology, 2020. **21**(5).
502 15. Balmas, E., et al., *Islet-autoreactive CD4+ T cells are linked with response to alefacept in type 1*
503 *diabetes.* JCI Insight, 2023. **8**(21).
504 16. Seay, H.R., et al., *Tissue distribution and clonal diversity of the T and B cell repertoire in type 1*
505 *diabetes.* JCI Insight, 2016. **1**(20): p. e88242.
506 17. Campbell-Thompson, M., et al., *Network for Pancreatic Organ Donors with Diabetes (nPOD):*
507 *developing a tissue biobank for type 1 diabetes.* Diabetes Metab Res Rev, 2012. **28**(7): p. 608-17.
508 18. Drotar, D.M., et al., *Impaired islet function and normal exocrine enzyme secretion occur with low*
509 *inter-regional variation in type 1 diabetes.* Cell Rep, 2024. **43**(6): p. 114346.
510 19. Shapiro, M.R., et al., *Human immune phenotyping reveals accelerated aging in type 1 diabetes.*
511 JCI Insight, 2023.
512 20. Subrahmanyam, P.B. and H.T. Maecker, *CyTOF Measurement of Immunocompetence Across*
513 *Major Immune Cell Types.* Curr Protoc Cytom, 2017. **82**: p. 9 54 1-9 54 12.

514 21. Crowell, H.L., et al., *An R-based reproducible and user-friendly preprocessing pipeline for CyTOF*
515 *data.* F1000Res, 2020. **9**: p. 1263.
516 22. Hahne, F., et al., *flowCore: a Bioconductor package for high throughput flow cytometry.* BMC
517 Bioinformatics, 2009. **10**: p. 106.
518 23. Phipson, B., et al., *propeller: testing for differences in cell type proportions in single cell data.*
519 Bioinformatics, 2022. **38**(20): p. 4720-4726.
520 24. McGinnis, C.S., L.M. Murrow, and Z.J. Gartner, *DoubletFinder: Doublet Detection in Single-Cell*
521 *RNA Sequencing Data Using Artificial Nearest Neighbors.* Cell Syst, 2019. **8**(4): p. 329-337 e4.
522 25. Mule, M.P., A.J. Martins, and J.S. Tsang, *Normalizing and denoising protein expression data from*
523 *droplet-based single cell profiling.* Nat Commun, 2022. **13**(1): p. 2099.
524 26. Hao, Y., et al., *Integrated analysis of multimodal single-cell data.* Cell, 2021. **184**(13): p. 3573-
525 3587 e29.
526 27. Borcherding, N., N.L. Bormann, and G. Kraus, *scRepertoire: An R-based toolkit for single-cell*
527 *immune receptor analysis.* F1000Res, 2020. **9**: p. 47.
528 28. Finak, G., et al., *MAST: a flexible statistical framework for assessing transcriptional changes and*
529 *characterizing heterogeneity in single-cell RNA sequencing data.* Genome Biol, 2015. **16**: p. 278.
530 29. Yu, G. and Q.Y. He, *ReactomePA: an R/Bioconductor package for reactome pathway analysis and*
531 *visualization.* Mol Biosyst, 2016. **12**(2): p. 477-9.
532 30. Borcherding, N., et al., *Mapping the immune environment in clear cell renal carcinoma by single-*
533 *cell genomics.* Commun Biol, 2021. **4**(1): p. 122.
534 31. Schattgen, S.A., et al., *Integrating T cell receptor sequences and transcriptional profiles by*
535 *clonotype neighbor graph analysis (CoNGA).* Nat Biotechnol, 2022. **40**(1): p. 54-63.
536 32. Perry, D.J., et al., *A genomic data archive from the Network for Pancreatic Organ donors with*
537 *Diabetes.* Sci Data, 2023. **10**(1): p. 323.
538 33. Wiedeman, A.E., et al., *Autoreactive CD8+ T cell exhaustion distinguishes subjects with slow type*
539 *1 diabetes progression.* Journal of Clinical Investigation, 2020. **130**(1).
540 34. Laban, S., et al., *Heterogeneity of circulating CD8 T-cells specific to islet, neo-antigen and virus in*
541 *patients with type 1 diabetes mellitus.* PLoS ONE, 2018. **13**(8).
542 35. Uno, S., et al., *Expression of chemokines, CXC chemokine ligand 10 (CXCL10) and CXCR3 in the*
543 *inflamed islets of patients with recent-onset autoimmune type 1 diabetes.* Endocr J, 2010.
544 **57**(11): p. 991-6.
545 36. Zhao, Y., et al., *Human CD8 T-stem cell memory subsets phenotypic and functional*
546 *characterization are defined by expression of CD122 or CXCR3.* Eur J Immunol, 2021. **51**(7): p.
547 1732-1747.
548 37. Chu, T., et al., *Precursors of exhausted T cells are pre-emptively formed in acute infection.*
549 Nature, 2025. **640**(8059): p. 782-792.
550 38. Chu, F., et al., *CXCR5(+)CD8(+) T cells are a distinct functional subset with an antitumor activity.*
551 Leukemia, 2019. **33**(11): p. 2640-2653.
552 39. Shapiro, M.R., et al., *Human immune phenotyping reveals accelerated aging in type 1 diabetes.*
553 JCI Insight, 2023. **8**(17).
554 40. Cao, C., X. Fu, and X. Wang, *Case Report: A novel mutation in TNFAIP3 in a patient with type 1*
555 *diabetes mellitus and haploinsufficiency of A20.* Front Endocrinol (Lausanne), 2023. **14**: p.
556 1131437.
557 41. Meixner, A., et al., *JunD regulates lymphocyte proliferation and T helper cell cytokine expression.*
558 EMBO J, 2004. **23**(6): p. 1325-35.
559 42. Bedford, J.G., et al., *Rapid interferon independent expression of IFITM3 following T cell activation*
560 *protects cells from influenza virus infection.* PLoS One, 2019. **14**(1): p. e0210132.

561 43. Kolumam, G.A., et al., *Type I interferons act directly on CD8 T cells to allow clonal expansion and*
562 *memory formation in response to viral infection.* J Exp Med, 2005. **202**(5): p. 637-50.
563 44. Tau, G.Z., et al., *Regulation of IFN-γ signaling is essential for the cytotoxic activity of CD8*
564 *T cells.* Journal of Immunology, 2001. **167**(10): p. 5574-5582.
565 45. Ng, D., et al., *A Lymphotoxin/Type I IFN Axis Programs CD8*
566 *T Cells To Infiltrate a Self-Tissue and Propagate Immunopathology.* Journal of Immunology, 2015.
567 **195**(10): p. 4650-4659.
568 46. Carow, B. and M.E. Rottenberg, *SOCS3, a Major Regulator of Infection and Inflammation.* Front
569 Immunol, 2014. **5**: p. 58.
570 47. Joosten, L.A., et al., *IL-32, a proinflammatory cytokine in rheumatoid arthritis.* Proc Natl Acad Sci
571 U S A, 2006. **103**(9): p. 3298-303.
572 48. Ciecko, A.E., et al., *Interleukin-27 Is Essential for Type 1 Diabetes Development and Sjogren*
573 *Syndrome-like Inflammation.* Cell Rep, 2019. **29**(10): p. 3073-3086 e5.
574 49. Jaiswal, H., et al., *The NF-kappaB regulator Bcl-3 restricts terminal differentiation and promotes*
575 *memory cell formation of CD8+ T cells during viral infection.* PLoS Pathog, 2021. **17**(1): p.
576 e1009249.
577 50. Sun, Q., et al., *BCL6 promotes a stem-like CD8(+) T cell program in cancer via antagonizing*
578 *BLIMP1.* Sci Immunol, 2023. **8**(88): p. eadh1306.
579 51. Seo, H., et al., *BATF and IRF4 cooperate to counter exhaustion in tumor-infiltrating CAR T cells.*
580 Nat Immunol, 2021. **22**(8): p. 983-995.
581 52. Ilangumaran, S., D. Bobbala, and S. Ramanathan, *SOCS1: Regulator of T Cells in Autoimmunity*
582 *and Cancer.* Curr Top Microbiol Immunol, 2017. **410**: p. 159-189.
583 53. Lu, D., et al., *The phosphatase PAC1 acts as a T cell suppressor and attenuates host antitumor*
584 *immunity.* Nature Immunology, 2020. **21**(3): p. 287-+.
585 54. Srirat, T., et al., *NR4a1/2 deletion promotes accumulation of TCF1(+) stem-like precursors of*
586 *exhausted CD8(+) T cells in the tumor microenvironment.* Cell Rep, 2024. **43**(3): p. 113898.
587 55. Yang, H., et al., *Stress-glucocorticoid-TSC22D3 axis compromises therapy-induced antitumor*
588 *immunity.* Nat Med, 2019. **25**(9): p. 1428-1441.
589 56. Cantor, J., et al., *Loss of T cell CD98hc specifically ablates T cell clonal expansion and protects*
590 *from autoimmunity.* Journal of Immunology, 2011. **186**.
591 57. Ng, S.S., et al., *The NK cell granule protein NKG7 regulates cytotoxic granule exocytosis and*
592 *inflammation.* Nat Immunol, 2020. **21**(10): p. 1205-1218.
593 58. Ravi, V.M., et al., *T-cell dysfunction in the glioblastoma microenvironment is mediated by*
594 *myeloid cells releasing interleukin-10.* Nature Communications, 2022. **13**(1).
595 59. Li, D., et al., *Intermediate Filament (IF) Protein Vimentin Regulates T Cell Mediated Immune*
596 *Response in Gvhd.* Blood, 2015. **126**(23).
597 60. Kollis, P.M., et al., *Characterising Distinct Migratory Profiles of Infiltrating T-Cell Subsets in*
598 *Human Glioblastoma.* Front Immunol, 2022. **13**: p. 850226.
599 61. Nagasaki, J., et al., *T cells with high BCL-2 expression induced by venetoclax impact anti-leukemic*
600 *immunity "graft-versus-leukemia effects".* Blood Cancer Journal, 2024. **14**(1).
601 62. Kurtulus, S., et al., *Bcl-2 allows effector and memory CD8+ T cells to tolerate higher expression of*
602 *Bim.* J Immunol, 2011. **186**(10): p. 5729-37.
603 63. Cao, C., et al., *CXCR4 orchestrates the TOX-programmed exhausted phenotype of CD8(+) T cells*
604 *via JAK2/STAT3 pathway.* Cell Genom, 2024. **4**(10): p. 100659.
605 64. Ray, A., et al., *Multimodal identification of rare potent effector CD8 T cells in solid tumors.*
606 bioRxiv, 2023.

607 65. Donato, R., *Functional roles of S100 proteins, calcium-binding proteins of the EF-hand type.*
608 Biochim Biophys Acta, 1999. **1450**(3): p. 191-231.
609 66. Zhu, W., et al., *A novel engineered IL-21 receptor arms T-cell receptor-engineered T cells (TCR-T*
610 *cells) against hepatocellular carcinoma.* Signal Transduct Target Ther, 2024. **9**(1): p. 101.
611 67. Ganes, S. and V. Fensterl, *Interferon-induced Ifit proteins: Their role in viral pathogenesis.*
612 Cytokine, 2015. **76**(1): p. 64-64.
613 68. Wang, Y., et al., *HLA-DR Expression Level in CD8(+) T Cells Correlates With the Severity of*
614 *Children With Acute Infectious Mononucleosis.* Front Immunol, 2021. **12**: p. 753290.
615 69. Lyngstadaas, A.V., et al., *Pro-Resolving Mediator Annexin A1 Regulates Intracellular Ca(2+) and*
616 *Mucin Secretion in Cultured Goblet Cells Suggesting a New Use in Inflammatory Conjunctival*
617 *Diseases.* Front Immunol, 2021. **12**: p. 618653.
618 70. Tu, Y., et al., *S100A11 functions as novel oncogene in glioblastoma via S100A11/ANXA2/NF-*
619 *kappaB positive feedback loop.* J Cell Mol Med, 2019. **23**(10): p. 6907-6918.
620 71. Ito, S., et al., *Accumulation of annexin A2 and S100A10 prevents apoptosis of apically*
621 *delaminated, transformed epithelial cells.* Proc Natl Acad Sci U S A, 2023. **120**(43): p.
622 e2307118120.
623 72. Su, L., et al., *Role of vimentin in modulating immune cell apoptosis and inflammatory responses*
624 *in sepsis.* Sci Rep, 2019. **9**(1): p. 5747.
625 73. Rao, L., D. Perez, and E. White, *Lamin proteolysis facilitates nuclear events during apoptosis.* J
626 Cell Biol, 1996. **135**(6 Pt 1): p. 1441-55.
627 74. Rocha-Perugini, V. and J.M. González-Granado, *Nuclear envelope lamin-A as a coordinator of T*
628 *cell activation.* Nucleus, 2014. **5**(5): p. 396-401.
629 75. Cui, A., et al., *Dictionary of immune responses to cytokines at single-cell resolution.* Nature,
630 2024. **625**(7994).
631 76. Lee, J., et al., *IL-15 promotes self-renewal of progenitor exhausted CD8 T cells during persistent*
632 *antigenic stimulation.* Front Immunol, 2023. **14**: p. 1117092.
633 77. Klebanoff, C.A., et al., *IL-15 enhances the in vivo antitumor activity of tumor-reactive CD8+ T*
634 *cells.* Proc Natl Acad Sci U S A, 2004. **101**(7): p. 1969-74.
635 78. Liang, T., et al., *Ex vivo human pancreatic slice preparations offer a valuable model for studying*
636 *pancreatic exocrine biology.* J Biol Chem, 2017. **292**(14): p. 5957-5969.
637 79. Marciniak, A., et al., *Using pancreas tissue slices for in situ studies of islet of Langerhans and*
638 *acinar cell biology.* Nat Protoc, 2014. **9**(12): p. 2809-22.
639 80. Huber, M.K., et al., *Beta Cell Dysfunction Occurs Independently of Insulitis in Type 1 Diabetes*
640 *Pathogenesis.* bioRxiv, 2024.
641 81. Sutherland, C.L., et al., *UL16-binding proteins, novel MHC class I-related proteins, bind to NKG2D*
642 *and activate multiple signaling pathways in primary NK cells.* J Immunol, 2002. **168**(2): p. 671-9.
643 82. Kirkham, C.L. and J.R. Carlyle, *Complexity and Diversity of the NKR-P1:Clr (Klrb1:Clec2)*
644 *Recognition Systems.* Front Immunol, 2014. **5**: p. 214.
645 83. Yoon, S.H., et al., *Selective addition of CXCR3(+) CCR4(-) CD4(+) Th1 cells enhances generation of*
646 *cytotoxic T cells by dendritic cells in vitro.* Exp Mol Med, 2009. **41**(3): p. 161-70.
647 84. Wang, Y., et al., *Characteristics of premanufacture CD8(+)T cells determine CAR-T efficacy in*
648 *patients with diffuse large B-cell lymphoma.* Signal Transduct Target Ther, 2023. **8**(1): p. 409.
649 85. Zhao, Y., et al., *An integrative analysis of the single-cell transcriptome identifies DUSP4 as an*
650 *exhaustion-associated gene in tumor-infiltrating CD8+T cells.* Functional & Integrative Genomics,
651 2023. **23**(2).
652 86. Patterson, A.R., et al., *Gimap5-dependent inactivation of GSK3β is required for CD4*

653 *T cell homeostasis and prevention of immune pathology.* Journal of Immunology, 2018. **200**(1).

654 87. Wang, Y.J., et al., *Multiplexed In Situ Imaging Mass Cytometry Analysis of the Human Endocrine*
655 *Pancreas and Immune System in Type 1 Diabetes.* Cell Metab, 2019. **29**(3): p. 769-783 e4.
656 88. Ackermann, A.M., et al., *Integration of ATAC-seq and RNA-seq identifies human alpha cell and*
657 *beta cell signature genes.* Mol Metab, 2016. **5**(3): p. 233-244.
658 89. Fasolino, M., et al., *Single-cell multi-omics analysis of human pancreatic islets reveals novel*
659 *cellular states in type 1 diabetes.* Nat Metab, 2022. **4**(2): p. 284-299.
660 90. Golden, G.J., et al., *Immune perturbations in human pancreas lymphatic tissues prior to and after*
661 *type 1 diabetes onset.* bioRxiv, 2024.
662 91. Coppieters, K.T., et al., *Demonstration of islet-autoreactive CD8 T cells in insulitic lesions from*
663 *recent onset and long-term type 1 diabetes patients.* J Exp Med, 2012. **209**(1): p. 51-60.
664 92. Vignali, D., et al., *Detection and characterization of CD8+ autoreactive memory Stem T cells in*
665 *patients with type 1 diabetes.* Diabetes, 2018. **67**(5).
666 93. Wang, Y.T., et al., *Stem cell-like memory T cells: The generation and application.* Journal of
667 Leukocyte Biology, 2021. **110**(6): p. 1209-1223.
668 94. Chen, J., et al., *Insulin-dependent diabetes induced by pancreatic beta cell expression of IL-15*
669 *and IL-15Rα.* Proceedings of the National Academy of Sciences of the United States of America,
670 2013. **110**(33): p. 13534-13539.
671 95. Kuczynski, S., et al., *IL-15 is elevated in serum patients with type 1 diabetes mellitus.* Diabetes
672 Research and Clinical Practice, 2005. **69**(3): p. 231-236.
673 96. Jacobsen, L.M., et al., *Responders to low-dose ATG induce CD4+ T cell exhaustion in type 1*
674 *diabetes.* JCI Insight, 2023. **8**(16).
675 97. Waibel, M., et al., *Baricitinib and beta-Cell Function in Patients with New-Onset Type 1 Diabetes.*
676 N Engl J Med, 2023. **389**(23): p. 2140-2150.
677 98. Perry, D.J., et al., *A genomic data archive from the Network for Pancreatic Organ donors with*
678 *Diabetes.* Scientific Data, 2023. **10**(1): p. 323.
679 99. Robertson, C.C., et al., *Fine-mapping, trans-ancestral and genomic analyses identify causal*
680 *variants, cells, genes and drug targets for type 1 diabetes.* Nat Genet, 2021. **53**(7): p. 962-971.
681 100. Perry, D.J., et al., *Application of a Genetic Risk Score to Racially Diverse Type 1 Diabetes*
682 *Populations Demonstrates the Need for Diversity in Risk-Modeling.* Sci Rep, 2018. **8**(1): p. 4529.
683 101. Mitchell, A.M., et al., *Tracking DNA-based antigen-specific T cell receptors during progression to*
684 *type 1 diabetes.* Sci Adv, 2023. **9**(49): p. eadj6975.
685 102. Tickotsky, N., et al., *McPAS-TCR: a manually curated catalogue of pathology-associated T cell*
686 *receptor sequences.* Bioinformatics, 2017. **33**(18): p. 2924-2929.
687 103. Vita, R., et al., *The Immune Epitope Database (IEDB): 2024 update.* Nucleic Acids Res, 2025.
688 **53**(D1): p. D436-D443.
689 104. Gao, S., et al., *Single-cell RNA sequencing coupled to TCR profiling of large granular lymphocyte*
690 *leukemia T cells.* Nat Commun, 2022. **13**(1): p. 1982.
691 105. Stadinski, B.D., et al., *Hydrophobic CDR3 residues promote the development of self-reactive T*
692 *cells.* Nat Immunol, 2016. **17**(8): p. 946-55.
693 106. Linsley, P.S., et al., *Germline-like TCR-α chains shared between autoreactive T cells in blood and*
694 *pancreas.* Nature Communications, 2024. **15**(1).
695 107. Christen, U., et al., *Combination treatment of a novel CXCR3 antagonist ACT-777991 with an*
696 *anti-CD3 antibody synergistically increases persistent remission in experimental models of type 1*
697 *diabetes.* Clin Exp Immunol, 2023. **214**(2): p. 131-143.
698 108. Boof, M.L., et al., *Pharmacokinetics, pharmacodynamics and safety of the novel C-X-C chemokine*
699 *receptor 3 antagonist ACT-777991: Results from the first-in-human study in healthy adults.* Br J
700 Clin Pharmacol, 2024. **90**(2): p. 588-599.

Tables

Table 1. Flow cytometry panel.

Antigen	Fluorophore	Clone	Manufacturer
CD197	BV421	G043H7	Biolegend
CD4	FITC	RPA-T4	BioLegend
CD45RA	PerCP-Cy5.5	HI100	BioLegend
CD185	PE	J252D4	BioLegend
CD183	PE-Cy7	G025H7	BioLegend
CD279	APC	eBioJ105	eBioscience
CD3	APC-H7	SK7	BD
Live/Dead	Live Dead Yellow	NA	Invitrogen

Table 2. Demographic information for mass cytometry (CyTOF) cohort.

Clinical Status	n	% Male	Age (yr)	% AAB+	Disease Duration (yr)	% Insulitis +	% High Risk HLA
T1D	10	80	19±6.5	90	6.5±7.4	90	100
ND	12	66.7	16.9±5.6	0	NA	0	66.7

*High Risk HLA was defined by possession of risk associated alleles: DRB1*0401,0402,0403,0404;DRB1*0301

Table 3. Demographic information for flow cytometry validation cohort.

Clinical Status	n	% Male	Age (yr)	# AAB	Disease Duration (yr)	% Insulitis +	% High Risk HLA
T1D	5	60	19.2±5.0	20% negative, 20% single, 20% double, 40% triple	10.5±9.8	80	100
AAB+	4	75	21.5±3.1	50% single, 50% double	NA	25	75
ND	15	66	17.1±7.1		NA	0	60

*High Risk HLA was defined by possession of risk associated alleles: DRB1*0401,0402,0403,0404;DRB1*0301

Table 4. Demographic information for scRNAseq cohort.

Clinical Status	n	% Male	Age (yr)	% AAB+	Disease Duration (yr)	% Insulitis+	% High Risk HLA
T1D	9	55	17.0±6.5	100	1.80±3.4	100	100
ND	7	71.4	17.1±3.1	0	NA	0	80

*High Risk HLA was defined by possession of risk associated alleles: DRB1*0401,0402,0403,0404;DRB1*0301

Table 5. Amino acid sequences of shared clones across pLN and pancreas slices.

Tissue(s)	Donor	Cluster(s)	Sequence	n
pLN, slice	6536	5,9	CAASIGFGNVLHC_CSSKKGLDEQFF	4
pLN	6551	0,2	CAVDSGGGADGLTF_CASSPAGAGYEQYF	4
pLN	6551	0,2	CAMRGPFRAGANNLFF_CSARGGPVSNEQFF	3
pLN, slice	6551	0,2	CASKTGANNLFF_CASAPGQGSEQLFF	3
pLN	6551	0,2	CAVKDNARLMF_CASSSGEAGTNSPLHF	3
pLN	6536	0,2	CAVRSPSLMDSNYQLIW_CASCRTGNYEQYF	3

723 **Figure Legends**

724 **Figure 1. Differential expression analysis of mass cytometry (CyTOF) data reveals enhanced CD8$^+$**
725 **CXCR3 expression in T1D pLN.** A) Experimental workflow involving processing of pancreatic lymph
726 node (pLN), staining for lineage, phenotypic, and quality control (QC) markers, and data collection
727 on a mass cytometer. After data acquisition, normalization of channels to internal bead controls
728 was performed using the premessa[21] package, and any confounding effects of batch or donor age
729 on cluster composition were accounted for in analysis through incorporation as covariates in a
730 linear model. B) UMAP of CD45$^+$ cells clustered at resolution 0.2 using Seurat. C) Heatmap
731 displaying Z-scored mean expression of markers for the clusters represented in (B), with dot size
732 representing percent of cells in the cluster expressing the marker, separated by ND (blue) and T1D
733 (orange) donor type. Cluster of interest is highlighted with the orange box. Asterisks mark
734 populations with significantly different expression by condition as determined by linear model with
735 batch as a covariate. D) Significantly increased cluster 4 (corresponding to naïve CD8$^+$ T cells) CXCR3
736 expression in T1D donors. P value refers to the FDR-corrected p value from the linear modeling.

737 **Figure 2. Differential abundance of CXCR3^{lo} naïve CD8 T cells in T1D pLN.** A) UMAP of subclustered
738 CD8$^+$ T cells. B) Z-scored DotPlot of marker expression for each CD8$^+$ T cell subcluster. C)
739 Significantly increased proportion of subcluster 0 (CXCR3^{lo} naïve like) in T1D pLN as determined by
740 linear modeling with donor age and CyTOF batch as covariates. D) Significantly increased
741 percentage of naïve CD8$^+$ T cells expressing CXCR3 found in an independent cohort of pLN donors
742 by flow cytometry. P value for (D) is the result of an ordinary one-way ANOVA with Tukey's multiple
743 test correction.

744 **Figure 3. IL-15 is predicted to drive signatures of memory maintenance and effector function in**
745 **T1D.** A) Experimental workflow for scRNAseq of pLN. B) UMAP projection of total pLN cells, which
746 were subsetted to T cells, reintegrated with rpca, and reclustered, resulting in 15 T cell clusters (C).
747 D) Heatmap of Z-scored gene expression data showing a selection of DEGs between T1D donors and
748 ND donors across naïve, Teff, and Texh $CD8^+$ T cells. E) Network plot using DEGs in naïve CD8 T cells
749 showing enrichment of reactome pathways in T1D. F) Network plot using DEGs in CD8 Teff cells
750 showing enrichment of reactome pathways in T1D. G) Network plot using DEGs in CD8 Texh cells
751 showing enrichment of reactome pathways in T1D. H) Compass plot of IREA results using the top
752 genes upregulated in T1D in naïve $CD8^+$ T cells ($p<0.05$, log2FC>0.26) as input. I) Compass plot of
753 IREA results using the top genes upregulated in T1D in $CD8^+$ Teff cells ($p<0.05$, log2FC>0.26) as
754 input. J) Compass plot of IREA results using the top genes upregulated in T1D in $CD8^+$ Texh cells
755 ($p<0.05$, log2FC>0.26) as input. H-J) Bar height is indicative of enrichment score, while color
756 corresponds to FDR-adjusted P-value (two-sided Wilcoxon rank-sum test). Genes highlighted on
757 heatmap (D) met log2FC cutoffs of 0.26 and adjusted p-value cutoffs of 0.05. Pathway analysis was
758 performed with the reactomePA package and visualized if adjusted $p<0.1$ with the clusterprofiler
759 package.

760 **Figure 4. Integrative receptor and gene expression analysis highlights an enriched naïve $CD8^+$ T**
761 **cell TCR cluster in T1D pLN.** A) schematic of CoNGA. B) UMAP of subsetted T cells colored by CoNGA
762 score (indicative of overlap in TCR and gene expression neighborhoods) and C) CoNGA gene
763 expression cluster, alongside D) CoNGA scores overlaid on the CoNGA TCR UMAP and E) TCR
764 clusters overlaid on the TCR UMAP. F) Increase in CoNGA GEX cluster 10 and TCR cluster 3 in T1D. G)
765 Gene expression and TCR Graph vs Graph results for CoNGA clusters with score <1. Left half of
766 semicircle indicates gene expression cluster, right half of semicircle indicates TCR cluster

767 assignment. Bar plots indicate the relative proportion of T1D (orange) and ND (blue) cells for the
768 given cluster (left) and for the entire dataset (right), followed by the same for nPOD ID, where each
769 color represents a different donor. Top 9 differentially expressed genes are shown per cluster, as
770 well as TCR genes, CDR3 motif logos, and TCR sequence features[31] (TCRseq features panel, with red
771 indicating higher and blue indicating lower scores relative to the rest of the dataset). A panel of
772 marker genes shown is shown on the far right with red dots colored by mean expression and sized
773 by percent of cells expressing the gene. Difference in cluster proportion assessed with two-way
774 Fisher's exact test.

775 **Figure 5. Tissue-dependent gene expression programs of memory CD8$^+$ T cell populations.** A)
776 Processing workflow of pancreatic slices where pancreas was embedded in agarose and sliced using
777 a vibratome to yield 150μm slices[78, 79], after which cells were processed to single cell suspension,
778 selected for CD45$^+$ cells, and run on the 10X Chromium controller as described in methods. B)
779 UMAP of integrated gene expression data (n=2 donors, pLN and pancreatic slices) illustrating
780 prevalence of clusters across tissues. C) Histological staining (obtained from nPOD Aperio e-slide
781 manager) of insulin (pink), glucagon (blue), and CD3 (brown) across pancreas tail of the two donors
782 with paired pancreatic slice and pLN data shows increased insulitis in new-onset donor 6551. Scale
783 bars are included in the upper left corner of each image and correspond to 10x magnification and
784 101um for donor 6551, and 20x magnification and 50um for donor 6536. D) Dotplot showing Z-
785 scored gene expression per cluster in (B), with dot size corresponding to percent of cells in the
786 cluster expressing the marker. E) Barplot illustrating distribution of expanded clones across clusters,
787 with the majority of expanded clones localizing to memory CD8$^+$ T cell clusters 0 (CD8 Teff) and 2
788 (CD8 cytotoxic T lymphocytes [CTL]). F) Assessment of repertoire overlap across tissues with the
789 Morisita-Horn metric shows limited sharing across tissues. G) Alluvial plot subsetted to only shared

790 clones showing clonal sharing between clusters 5 (eTreg) and 9 (ICOS^{hi} TCM), and 0 (CD8 Teff) and 2
791 (CD8 CTL) across both clusters and tissues. H) Barplot of percent of each cluster per tissue illustrates
792 differential subset abundance of innate and adaptive immune cells. I) Violin plots illustrating
793 differential expression of *LEF1* and *SELL* in CD8 T cells between tissues. J) Volcano plot of
794 differentially expressed genes in cluster 0 (CD8 Teff) between pancreatic slices and pLN. K) Volcano
795 plot of differentially expressed genes in cluster 2 (CD8 CTL) between pancreatic slices and pLN.
796 DEGs were defined as log2FC>0.26 and corrected p value<0.05. L) GSEA analysis of cluster 0 using
797 Hallmark genesets. M) GSEA analysis of cluster 2 using Hallmark genesets. GSEA analysis was
798 performed using escape, and DE genesets were identified with a Wilcoxon test. The top 20 gene
799 sets with adjusted p <0.05 were plotted with positive fold change indicating upregulation in
800 pancreatic slice (orange) and negative fold change indicating upregulation in pLN (blue).

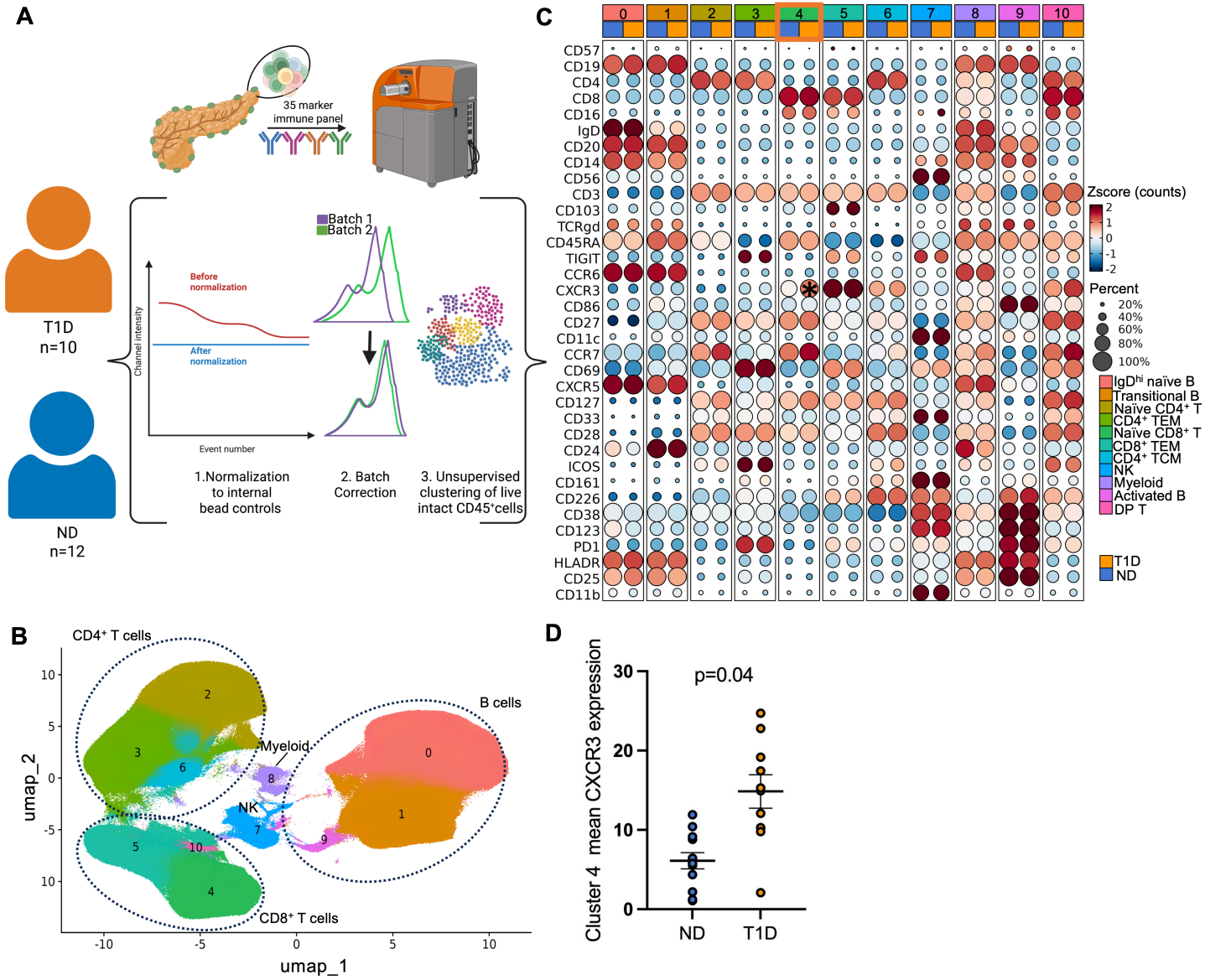
A
35 marker immune panel
T1D
n=10
ND
n=12
Batch 1
Batch 2
Before normalization
After normalization
Channel intensity
Event number
1.Normalization to internal bead controls
2. Batch Correction
3. Unsupervised clustering of live intact CD45⁺cells
C
0
1
2
3
4
5
6
7
8
9
10
CD57
CD19
CD4
CD8
CD16
IgD
CD20
CD14
CD56
CD3
CD103
TCRgd
CD45RA
TIGIT
CCR6
CXCR3
CD86
CD27
CD11c
CCR7
CD69
CXCR5
CD127
CD33
CD28
CD24
ICOS
CD161
CD226
CD38
CD123
PD1
HLADR
CD25
CD11b
Zscore (counts)
2
1
0
-1
-2
Percent
20%
40%
60%
80%
100%
IgDhi naïve B
Transitional B
Naïve CD4⁺ T
CD4⁺ TEM
Naïve CD8⁺ T
CD8⁺ TEM
CD4⁺ TCM
NK
Myeloid
Activated B
DP T
T1D
ND
B
CD4⁺ T cells
B cells
Myeloid
NK
CD8⁺ T cells
umap_2
umap_1
D
p=0.04
Cluster 4 mean CXCR3 expression
ND
T1D

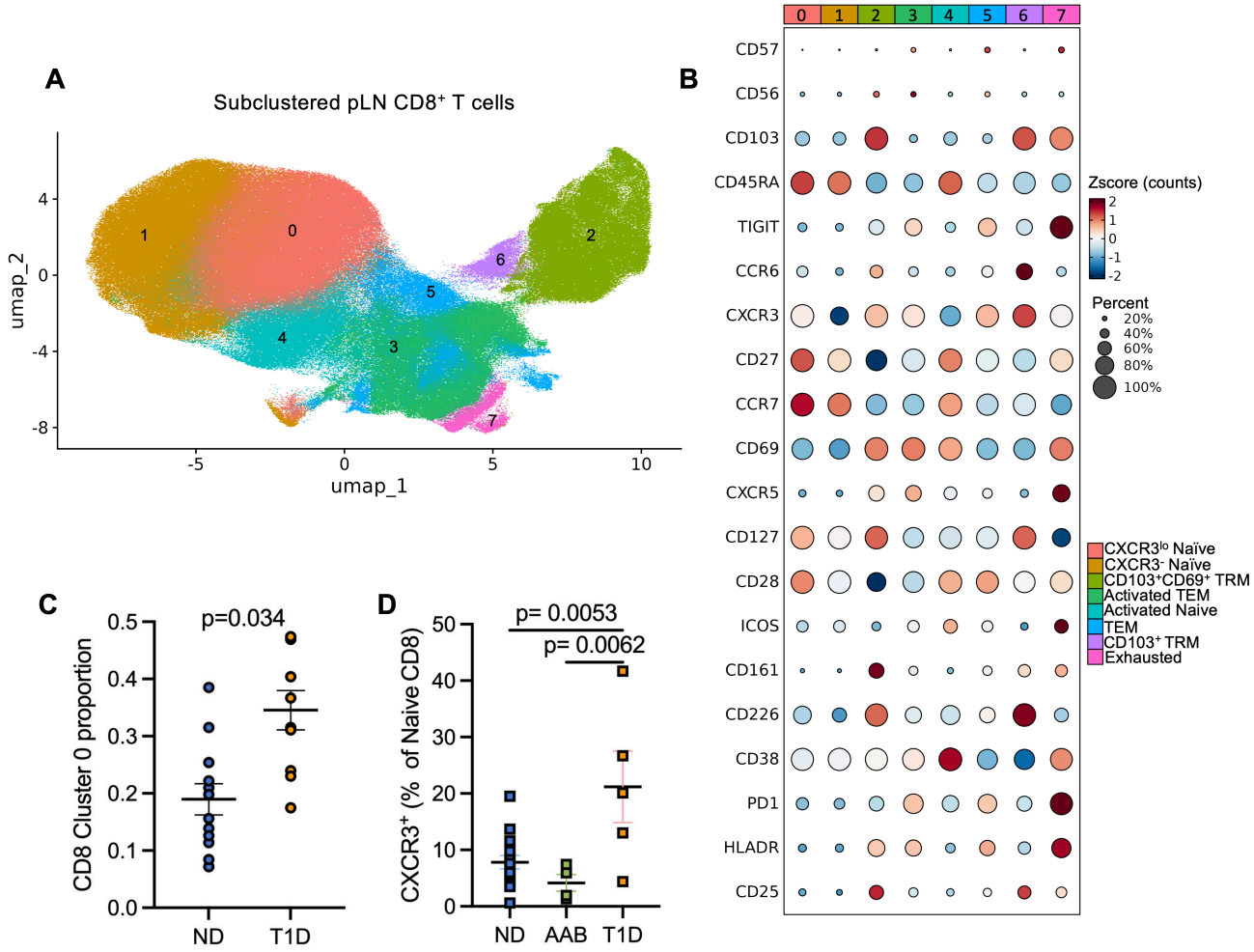
A
Subclustered pLN CD8⁺ T cells
umap_2
umap_1
0
1
2
3
4
5
6
7
B
CD57
CD56
CD103
CD45RA
TIGIT
CCR6
CXCR3
CD27
CCR7
CD69
CXCR5
CD127
CD28
ICOS
CD161
CD226
CD38
PD1
HLADR
CD25
Zscore (counts)
Percent
20%
40%
60%
80%
100%
CXCR3lo Naïve
CXCR3- Naïve
CD103+CD69+ TRM
Activated TEM
Activated Naive
TEM
CD103+ TRM
Exhausted
C
p=0.034
CD8 Cluster 0 proportion
ND
T1D
D
p= 0.0053
p= 0.0062
CXCR3+ (% of Naive CD8)
ND
AAB
T1D

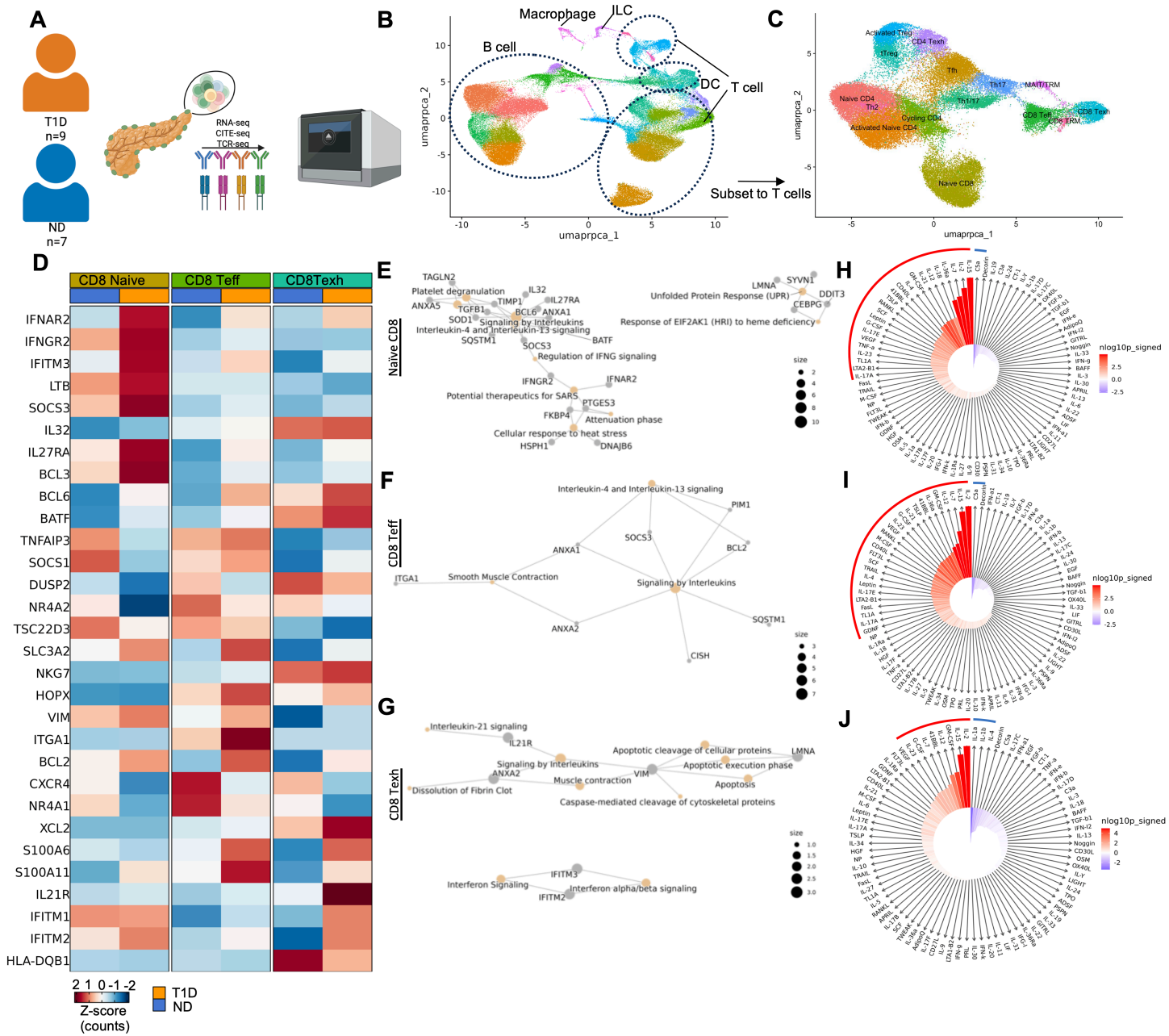
A
T1D
n=9
ND
n=7
RNA-seq
CITE-seq
TCR-seq
B
Macrophage
ILC
B cell
DC
T cell
umaprpca_2
umaprpca_1
Subset to T cells
C
Activated Treg
CD4 Texh
Tfh
Th17
MAIT/TRM
Th1/17
Naive CD4
Th2
Cycling CD4
Activated Naive CD4
CD8 Teff
CD8 Texh
CD8 TRM
Naive CD8
D
CD8 Naive
CD8 Teff
CD8Texh
IFNAR2
IFNGR2
IFITM3
LTB
SOCS3
IL32
IL27RA
BCL3
BCL6
BATF
TNFAIP3
SOCS1
DUSP2
NR4A2
TSC22D3
SLC3A2
NKG7
HOPX
VIM
ITGA1
BCL2
CXCR4
NR4A1
XCL2
S100A6
S100A11
IL21R
IFITM1
IFITM2
HLA-DQB1
Z-score
(counts)
T1D
ND
E
Naive CD8
TAGLN2
Platelet degranulation
ANXA5
TGFB1
TIMP1
IL32
IL27RA
BCL6
ANXA1
SOD1
Signaling by Interleukins
Interleukin-4 and Interleukin-13 signaling
SQSTM1
SOCS3
BATF
Regulation of IFNG signaling
IFNGR2
IFNAR2
Potential therapeutics for SARS
PTGES3
FKBP4
Attenuation phase
Cellular response to heat stress
HSPH1
DNAJB6
LMNA
SYVN1
Unfolded Protein Response (UPR)
DDIT3
CEBPG
Response of EIF2AK1 (HRI) to heme deficiency
size
F
CD8 Teff
Interleukin-4 and Interleukin-13 signaling
PIM1
SOCS3
ANXA1
BCL2
ITGA1
Smooth Muscle Contraction
Signaling by Interleukins
SQSTM1
ANXA2
CISH
size
G
CD8 Texh
Interleukin-21 signaling
IL21R
Apoptotic cleavage of cellular proteins
LMNA
Signaling by Interleukins
ANXA2
Apoptotic execution phase
VIM
Muscle contraction
Apoptosis
Dissolution of Fibrin Clot
Caspase-mediated cleavage of cytoskeletal proteins
Interferon Signaling
IFITM3
Interferon alpha/beta signaling
IFITM2
size
H
I
J
nlog10p_signed

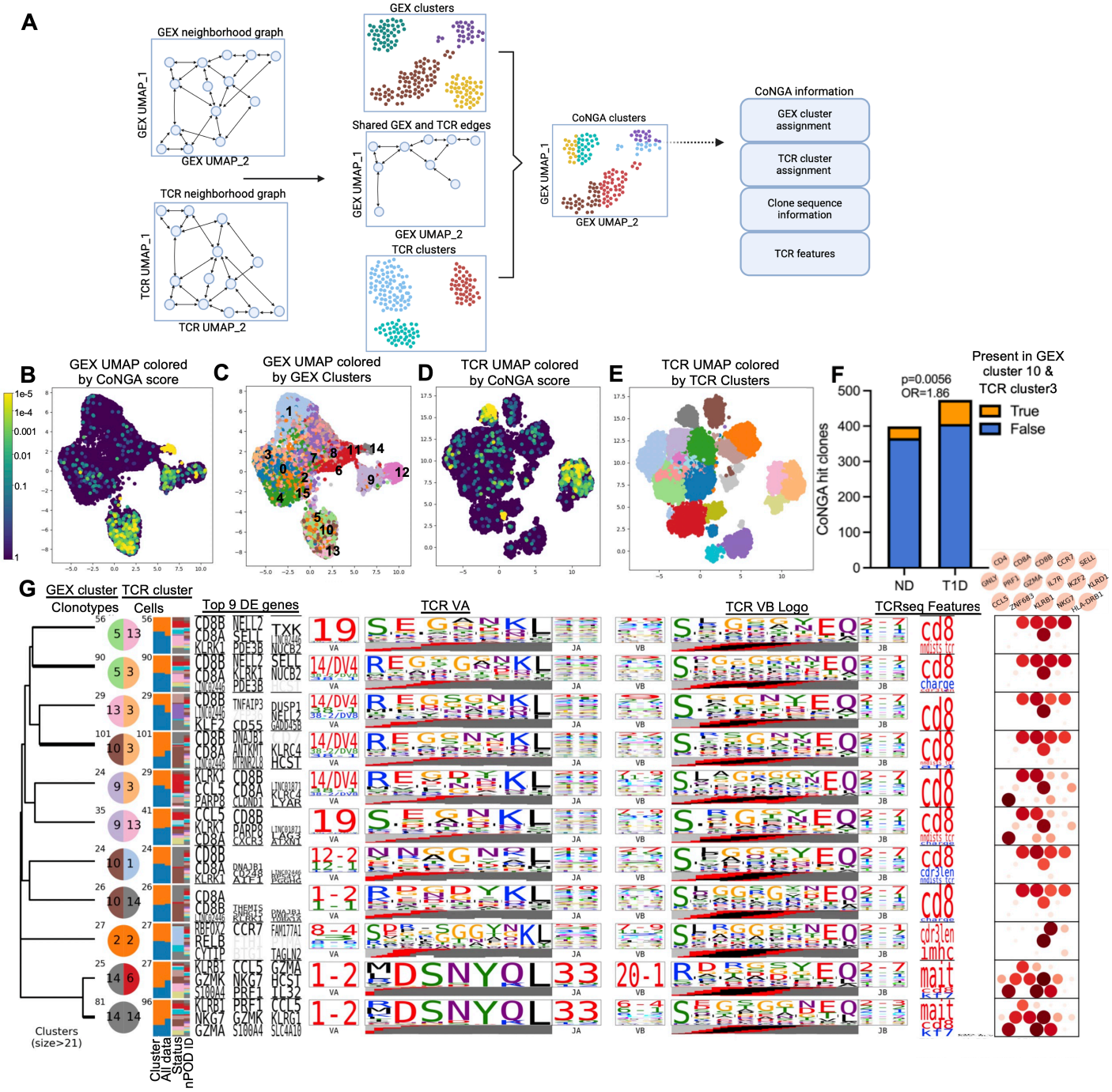
A
GEX neighborhood graph
GEX UMAP_1
GEX UMAP_2
TCR neighborhood graph
TCR UMAP_1
TCR UMAP_2
GEX clusters
Shared GEX and TCR edges
TCR clusters
CoNGA clusters
CoNGA information
GEX cluster assignment
TCR cluster assignment
Clone sequence information
TCR features
B
GEX UMAP colored by CoNGA score
C
GEX UMAP colored by GEX Clusters
D
TCR UMAP colored by CoNGA score
E
TCR UMAP colored by TCR Clusters
F
Present in GEX cluster 10 & TCR cluster3
p=0.0056
OR=1.86
True
False
CoNGA hit clones
ND
T1D
G
GEX cluster
TCR cluster
Clonotypes
Cells
Top 9 DE genes
TCR VA
TCR VB Logo
TCRseq Features
Clusters (size>21)
Cluster
All data
Status
nPOD ID

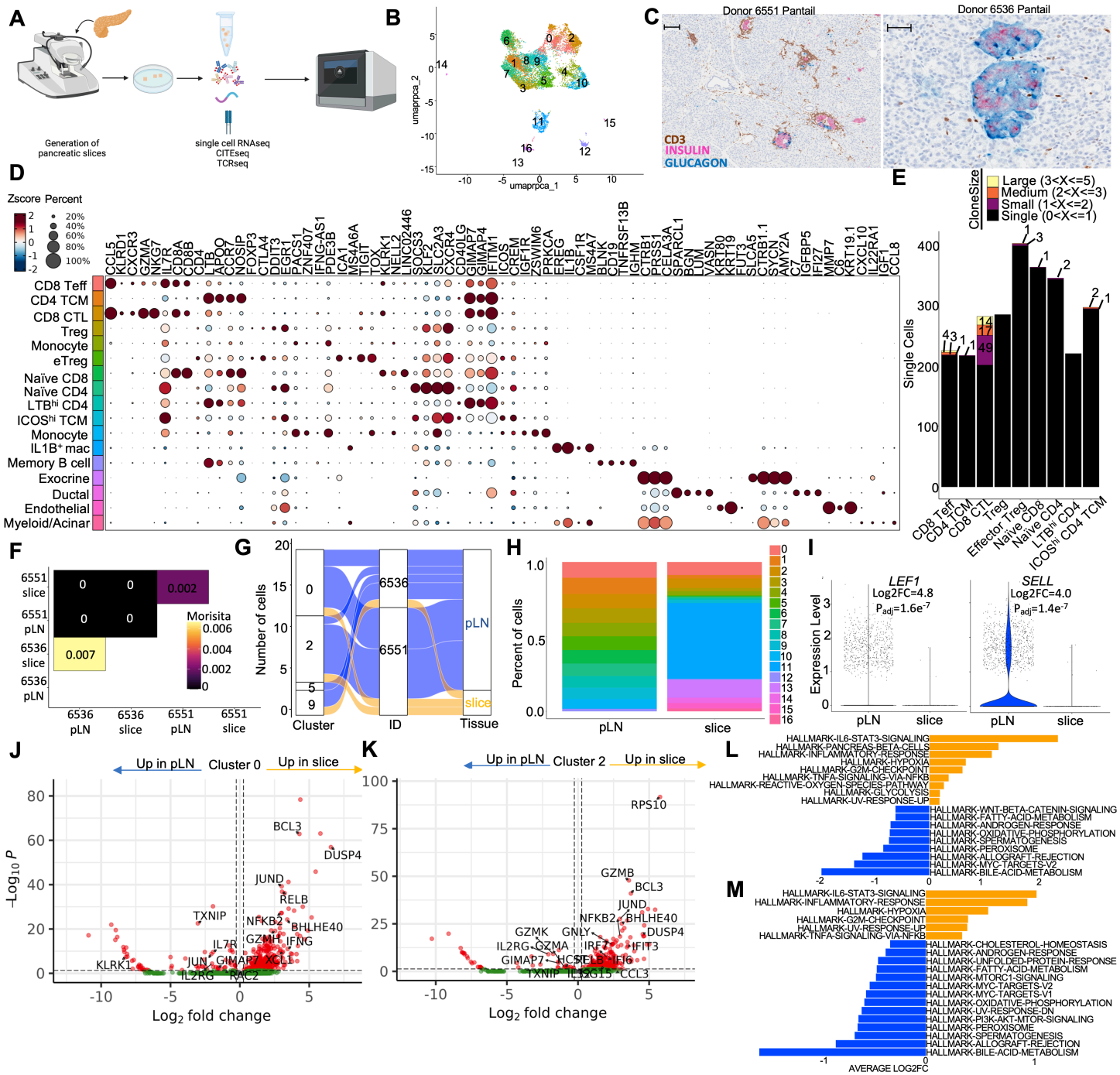
A
Generation of pancreatic slices
single cell RNAseq
CITEseq
TCRseq
B
umaprpca_1
umaprpca_2
C
Donor 6551 Pantail
Donor 6536 Pantail
CD3
INSULIN
GLUCAGON
D
Zscore Percent
CD8 Teff
CD4 TCM
CD8 CTL
Treg
Monocyte
eTreg
Naïve CD8
Naïve CD4
LTBhi CD4
ICOShi TCM
Monocyte
IL1B+ mac
Memory B cell
Exocrine
Ductal
Endothelial
Myeloid/Acinar
E
CloneSize
Large (3<X<=5)
Medium (2<X<=3)
Small (1<X<=2)
Single (0<X<=1)
Single Cells
CD8 Teff
CD4 TCM
CD8 CTL
Treg
Effector Treg
Naïve CD8
Naïve CD4
LTBhi CD4
ICOShi CD4 TCM
F
Morisita
6551 slice
6551 pLN
6536 slice
6536 pLN
G
Number of cells
Cluster
ID
Tissue
pLN
slice
H
Percent of cells
pLN
slice
I
LEF1
Log2FC=4.8
Padj=1.6e-7
SELL
Log2FC=4.0
Padj=1.4e-7
Expression Level
pLN
slice
J
Up in pLN
Cluster 0
Up in slice
Log2 fold change
K
Up in pLN
Cluster 2
Up in slice
Log2 fold change
L
M
AVERAGE LOG2FC